Evaluation of interfacial strength between fiber and matrix based on cohesive zone modeling

Bentang Arief Budiman[a], Kosuke Takahashi[b,*], Kazuaki Inaba[c], Kikuo Kishimoto[c]

[a]Mechanical Engineering Department, Institut Teknologi Bandung,
Ganesha street no. 10, Bandung 40132, Indonesia

[b]Division of Mechaical and Aerospace Engineering, Hokkaido University,
N13, W8, Kita-ku, Sapporo, Hokkaido, 060-8628, Japan

[c]Department of Transdisciplinary Science and Engineering, Tokyo Institute of Technology, 2-12-1 I6-10, Ookayama, Meguro-ku, Tokyo 152-8552, Japan

*E-mail: ktakahashi@eng.hokudai.ac.jp

Abstract

This paper presents a measurement technique of interfacial strength considering non-rigid bonding on a fiber/matrix interface modeled as a cohesive surface. By focusing on the stress concentration near a fiber crack obtained from a single-fiber fragmentation test, the stress contours in matrix observed by photoelasticity can be related to the interfacial strength by defining a characteristic length. An equation expressing the relationship between the characteristic length on the stress contour and the interfacial strength was derived, and validated using finite element analysis. The primary advantage of proposed measurement technique is that only a single fiber crack, which usually occurs within elastic deformation of matrix, is required for the evaluation of interfacial strength, whereas saturated fiber fragmentation is necessary in the conventional method. Herein, a sample application was demonstrated using a single carbon fiber and epoxy specimen, and an average interfacial strength of 23.8 MPa was successfully obtained.

Keywords

B. Interface/interphase, B. Fragmentation, B. Fiber/matrix bond, C. Cohesive interface modelling

1. Introduction

The interface between fiber and matrix plays an important role in the overall load-bearing performance of the composite structure. In particular, the bonding quality of the interface determines the stress transfer from the matrix to the fiber and vice versa [1, 2]. The bonding quality of the interface has been assessed through the development of interface models. An early model representing stress transfer at an interface was introduced by Cox and Kelly-Tyson [3, 4]. Kim et al. then modified this model by introducing the bonding quality parameter, i.e., the interfacial strength (t_o) was regarded as the stress required to initiate an interfacial crack [5]. Moreover, the bonding quality has also been determined using energy-based approaches [6–8].

The similarity between the abovementioned models is that the interface is assumed to be a two-dimensional surface with a rigid bonding condition. However, recent studies have shown that the interface is, in fact, a three-dimensional thin layer (also called an interphase) having mechanical properties that are different from those of both the fiber and the matrix [9–11]. Several studies have indicated that non-rigid bonding is formed at the interface regardless of the strength of the bonding condition [12–14]. Therefore, earlier models may have evaluated the bonding quality inaccurately [15, 16].

Recently, a surface-based cohesive model that defines the interface as a non-rigid bond has been attracting attention [17–19]. It provides an improved interpretation of the real interface condition by introducing the traction (t) - separation (δ) curve. However, characterization of the maximum traction, which is equivalent to t_o, from the t - δ curve has not been well established because it is difficult to experimentally measure the t - δ curve along the interface [20]. Among familiar experimental methods of push-out testing [21], micro bond testing [22], and single fiber fragmentation testing (SFFT) [23], SFFT is appropriate to consider the interface as a non-rigid bond because it replicates actual stress transfer in real fiber/matrix composites. It also has an advantage of the easier preparation of specimens [24, 25]. Our group previously proposed a method based on SFFT for evaluating t_o without requiring the t - δ curve observation [26]. It utilizes contours of principal stress difference ($\Delta\sigma$) in a matrix by defining a characteristic length (L_t), which can be obtained directly via photoelastic analysis [27-29]. Moreover, our method requires only a single fiber crack in the specimen whereas conventional SFFT requires complete fiber cracks generated until saturation. Thus, the influence of plastic deformation on the matrix can be significantly reduced.

This paper introduces a theoretical analysis of $\Delta\sigma$ contours to establish a novel technique of evaluating t_o at the debonding interface. First, an equation showing the relationship between the $\Delta\sigma$ contour and t_o is derived from the stress distribution of the matrix near the fiber crack during SFFT. FEA is then conducted to examine the derived equation. The application of L_t for the measurement of t_o is finally demonstrated using a carbon fiber/epoxy sample. A photoelastic image representing the $\Delta\sigma$ concentration in the matrix is analyzed by an image processing technique [30], to determine t_o from the L_t value using the derived equation.

2. Theory

2.1. Surface-based cohesive model for interface

Strain (ε_a) was imposed on a SFFT specimen consisting of a single fiber surrounded by a matrix to initiate fiber fragmentation, as shown in Figs. 1a and 1b. Shear traction (t_s) and separation (δ_s) developed in the interface soon after a fiber crack was generated, and then increased in response to the applied ε_a. When the relationship between t_s and δ_s is assumed to be simply expressed by the t_s –δ_s curve as shown in Fig. 2, three interfacial properties can be defined: interfacial stiffness (K_o), t_o, and the interfacial fracture toughness (G_c). K_o is a parameter that relates t_s and δ_s in a bonding condition, where

$$t_s = K_o \delta_s. \tag{1}$$

The real interface condition can be more suitably represented by the definition of K_o than the assumption of rigid bonding, because it implies that the interface can undergo separation even though t_s does not exceed t_o. Here, t_o is defined as the t_s required to initiate the debonding process, represented by degradation of K_o. Further, G_c, which can be obtained from the total area below the t_s – δ_s curve, is defined as the energy release rate required to cause debonded interface.

The position on the interface where t_s reaches a maximum can be found by examining the stress distribution in the matrix. Although it is difficult to observe the t_s distribution along the interface directly, t_o can be obtained by observing the $\Delta\sigma$ contour near the interface. It simply corresponds to the point of maximum $\Delta\sigma$ because $\Delta\sigma$ is a representative of principal shearing stress. Therefore, $\Delta\sigma$ can be an indicator of the maximum t_s, which is equal to t_o.

In order to confirm the relationship between t_s and the $\Delta\sigma$ contour, FEA using Abaqus 6.14 was conducted for an axisymmetric model, as shown in Fig. 3. It represents a region near a fiber crack, indicated by the dashed line in Fig. 1b. The single fiber and matrix were assumed to be linearly elastic materials, because the first fiber crack usually appears in the elastic range of the matrix. The mechanical properties of the fibers and matrices used in the FEA are shown in Table 1. The model geometry and the number of elements are shown in Table 2. Three sample cases with the different interfacial properties shown in Table 3 were examined. The range of t_o was determined based on previous study [9]. The values of G_c and K_o were suitably selected so that FEA calculation converges under ε_a of less than 3%, which is comparable to experimental results. Note that stress state of matrix for SFFT can be represented by axisymmetric model because of low volume fraction of fiber ($a << b$) even though the actual cross section of SFFT specimen is not axisymmetric [26, 31].

Fig. 4a shows the t_s and dt_s/dz distribution along the interface obtained from a simulation result for a carbon fiber-hard epoxy composite with case-1 interfacial properties in Table 3. The t_s becomes maximum value of 30 MPa, which is identical to t_o defined in case-1, at the boundary (z_o) between the bonded and debonding regions. It almost linearly decreases in the bonded region, resulting in almost constant dt_s/dz near the fiber crack. The $\Delta\sigma$ contours in the matrix shown in Fig. 4b clearly show that t_o causes a highly concentrated $\Delta\sigma$ near the fiber crack. The black points on each contour in Fig. 4b indicate the positions located farthest from the interface, represented by the maximum radius (r_{max}). Subtracting the fiber radius (a), it can be used as an indicator of t_o since our previous work found a linear relationship between them [26]. Therefore, it was defined as a characteristic length, L_t.

$$L_t = r_{max} - a \tag{2}$$

Among the contours in Fig. 4b, those with a $\Delta\sigma$ of 50 MPa or higher are ideal to find the maximum t_s, because the location of L_t corresponds well to the z_o. The L_t-based approach is not effective when the $\Delta\sigma$ contours are far from the interface because the maximum radius on contours gradually shift to the left due to the edge effects of the calculation area.

2.2. Equation relating L_t and t_o

The equation relating L_t and t_o is derived by the $\Delta\sigma$ equation from stress state in the bonding region near the interface ($z \geqq z_0$) where the deformations of matrix is linearly elastic. It is expressed by the axial (σ_z), radial (σ_r), and shear stress on the rz axis (τ_{rz}).

$$\frac{\Delta\sigma}{2} = \sqrt{\left(\frac{1}{2}(\sigma_z - \sigma_r)\right)^2 + \tau_{zr}^2} \tag{3}$$

In an axisymmetric model of the bonding region, the above stresses are related with hoop stress (σ_θ) and axial displacement (u_z) by equilibrium and the stress-strain relations for perfectly elastic and isotropic matrices.

$$\frac{\partial\sigma_z}{\partial z} + \frac{\tau_{rz}}{r} + \frac{\partial\tau_{rz}}{\partial r} = 0 \tag{4}$$

$$\frac{\partial\sigma_r}{\partial r} + \frac{\partial\tau_{rz}}{\partial z} + \frac{1}{r}(\sigma_r - \sigma_\theta) = 0 \tag{5}$$

$$\frac{\partial u_z}{\partial z} = \frac{1}{E}[\sigma_z - v(\sigma_r + \sigma_\theta)] \tag{6}$$

$$\frac{\partial u_z}{\partial r} = \frac{2(1+v)}{E}\tau_{rz} \tag{7}$$

where E and v are the elastic modulus and Poisson ratio, respectively. It should be noted that the radial displacement (u_r) was assumed to be zero near the interface because a is very small compared with the matrix radius (b). The boundary conditions of the matrix model shown in Fig. 3 are expressed as

$$\tau_{rz}(a,z) = t_s\ ;\ \tau_{rz}(b,z) = 0, \tag{8}$$

$$\sigma_r(a,z) = -q\ ;\ \sigma_r(b,z) = 0, \tag{9}$$

$$u_z(b, z) = \varepsilon_a z, \tag{10}$$

where q is the stress due to the Poisson ratio difference of the fiber and matrix. This can be calculated from the following equation [32].

$$q = \frac{\varepsilon_a\left(v_m - v_f\right)}{\left(\frac{1-v_f-2v_f^2}{E_f}\right) + \left(\frac{1+v_m}{E_m}\right)}, \tag{11}$$

where f and m refer to the fiber and matrix, respectively.

Intensive studies have been conducted by Zhao et al. and Nair et al. regarding the decay function of τ_{rz} along r axis [31, 33]. These studies have shown that, for a very low fiber-volume fraction model ($a << b$) such as in the case of an SFFT specimen, the simplest τ_{rz} that satisfies Eq. 4 and the boundary condition of Eq. 8 became the following equation.

$$\tau_{rz} = \frac{a}{r} t_s \tag{12}$$

Here, the t_s is assumed to be a linear function of z based on the FEA result shown in Fig. 4a. Considering a constant value of dt_s/dz near the fiber crack, the radial and hoop stresses can be obtained from Eq. 5 with the boundary conditions of Eq. 9 under the assumption of uniform axial stress along z direction and low fiber-volume fraction ($a <<$ b) .

$$\sigma_r = -\frac{a^2}{r^2} q \tag{13}$$

$$\sigma_\theta = \frac{a^2}{r^2} q + a\frac{dt_s}{dz} \tag{14}$$

The σ_z is derived by obtaining u_z from Eqs. 6 and 7, and then substituting the stresses of Eqs. 12, 13, and 14.

$$\sigma_z = E_m \varepsilon_a + a\frac{dt_s}{dz}\left(v_m + 2(1+v_m)\ln\frac{r}{b}\right) \tag{15}$$

It is reasonable that the σ_r, σ_θ, and σ_z, are only functions of r (uniform along z direction) because they actually have little effect to the overall stress state compared with shear stress. Substituting Eqs. 12, 13, and 15 into Eq. 3, t_s can be expressed as a function of $\Delta\sigma$ and the distance from the interface to the $\Delta\sigma$ contour (r).

$$t_s = \frac{r}{2a}\sqrt{\Delta\sigma^2 - \left(E_m\varepsilon_a + a\frac{dt_s}{dz}\left(v_m + 2(1+v_m)\ln\frac{r}{b}\right) + \frac{a^2}{r^2}q\right)^2} \qquad (16)$$

Focusing on the maximum radius on a $\Delta\sigma$ contour near the interface, where $r = L_t + a$ and $t_s = t_o$, t_o can be expressed in terms of L_t.

$$t_o = \frac{(L_t + a)}{2a}\sqrt{\Delta\sigma^2 - \left(E_m\varepsilon_a + a\frac{dt_s}{dz}\left(v_m + 2(1+v_m)\ln\frac{L_t + a}{b}\right) + \frac{a^2}{(L_t + a)^2}q\right)^2} \qquad (17)$$

Further, the constant dt_s/dz parameter must be obtained to apply Eq. 17 for evaluating t_0, but it is difficult to theoretically derive the value. Therefore, FEM results were utilized to estimate dt_s/dz parameter. As an example of t_s and dt_s/dz distributions along the interface shown in Fig. 4a, dt_s/dz = -249 MPa/mm at a point of t_o = 30 MPa was obtained by approaching from the bonding region. TheL_t values corresponding to $\Delta\sigma$ contours between 40 and 65 MPa were then measured and substituted into Eq. 17 in order to obtain t_o. The same procedure was repeated for other parameters in Table 3.

Results were calculated for both the carbon fiber/hard epoxy and glass fiber/soft epoxy models, and are plotted in Figs. 5 and 6, respectively. The dashed lines indicate the actual t_o input in the FEA, whereas the data-points indicate the estimated t_o using Eq. 17 with L_t and dt_s/dz values. Measurements excluding dt_s/dz effect (dt_s/dz = 0) are also plotted here, because it has been neglected in a large number of theoretical analyses due to simplification [5–10]. These figures clearly show that more accurate t_o values are obtained when dt_s/dz is included in the equation. Specifically, t_o values are overestimated when dt_s/dz is neglected. These results show that t_o can be accurately evaluated by measuring L_t. Moreover, these findings indicate that the assumptions applied in the derivation of Eq. 17 are reasonable and yield good agreement with the FEA results.

2.3. Non-dimensional analysis for practical use

Although Eq. 17 produces good results regarding evaluation of t_o, it is not practically useful if FEA must be conducted to obtain dt_s/dz parameter. Therefore, Eq. 17 was rearranged to a non-dimensional form to identically evaluate dt_s/dz term. Both sides of Eq. 17 were divided by $\Delta\sigma$ in order to obtain a general form that is independent of material properties.

$$t' = \frac{(L' + 1)}{2}\sqrt{1 - \left(\frac{E_m \varepsilon_a}{\Delta\sigma} + \frac{a}{\Delta\sigma}\frac{dt_s}{dz}\left(v_m + 2(1 + v_m)\ln\frac{a(L' + 1)}{b}\right) + \frac{1}{(L' + 1)^2}\frac{q}{\Delta\sigma}\right)^2} \quad (18)$$

where $t' = t_o/\Delta\sigma$ and $L' = L_t/a$.

The relationship between t' and L' is plotted in Eq. 18 for both the carbon fiber/hard epoxy and glass fiber/soft epoxy models. It was found that the relationship is identical regardless of materials and can be approximated by a simple linear equation, which was implied in our previous work [26].

$$t_0 = \left(0.21\frac{L_t}{a} + 0.45\right)\Delta\sigma \quad (19)$$

Through a linear approximation of Eq. 18, expressed by Eq. 19, the dt_s/dz value is no longer required for the t_o estimation. By selecting the appropriate $\Delta\sigma$ contour, which should be as close as possible to the interface, and by measuring L_t from the SFFT experiment, the t_o can be evaluated directly. Thus, Eq. 19 contributes significantly towards the effective and efficient measurement of t_o. Moreover, it can be applied to any relationship of t_s –δ_s curve on the interface since our proposed method only focuses on the location of z_o.

3. Experiment

3.1. Experimental procedure

SFFT was conducted to estimate t_o by proposed method of L_t measurement. Single carbon fiber (HTS30 3K, TOHO Tenax) and epoxy resin (KONISHI Chemical Co., Ltd.) were prepared to create an SFFT specimen with 2-mm thickness (h). The experimental setup consists of a polychromatic light and a microscope with a digital camera attached. A micro-tensile testing machine was located under the microscope so that the specimen was placed at the center of two polarizers. The retarders were also used to create circularly polarized light for the elimination of isoclinic and isochromatic interaction noise. A detailed schematic of the apparatus is shown in Fig. 8.

Stress contours can be observed because epoxy has two refraction indexes, as it is a birefringence material. The presence of two refraction indexes generates relative retardation expressed in the fringe order (N). Thus, N indicates $\Delta\sigma$, which is connected to the stress-optic coefficient (f_σ).

$$\Delta\sigma = \frac{f_\sigma N}{h} \tag{20}$$

First, f_σ of the pure-epoxy specimen, meaning no carbon fiber embedded, was obtained from a bending test [34]. $\Delta\sigma$ distribution under bending load and an image of continuous colored band corresponding to N can be simultaneously recorded. f_σ was then calculated by using Eq. 20. Next, ε_a was applied to a specimen of single fiber-embedded epoxy to capture the $\Delta\sigma$ contours near the fiber crack. On a certain ε_a, a fiber crack appeared and caused a $\Delta\sigma$ concentration near the interface. An image of colors corresponding to $\Delta\sigma$ contours was then captured by the camera through the microscope, and then the colors were extracted and converted to hue-saturation-value (HSV) system values. The conversion of colors to these values eliminates errors in color comparison, so that accurate results can be assured. Finally, L_t was measured from the $\Delta\sigma$ contours near the interface, and applied to Eq. 19 to obtain t_o.

3.2. Results and Discussion

Fig. 9a shows captured color image from bending test correspond to N with bending load of 6.2 N. The black color band in the specimen indicates no stress. Focusing on tensile stress distribution in the upper side of specimen, the $\Delta\sigma$ - N curve of the epoxy, shown in Fig. 9b, indicated that the f_σ of the epoxy specimen was 7.9 MPa.mm. The E_m of 0.67 GPa was also obtained from a tensile test.

On the SFFT, a fiber crack appeared at the ε_a of a 1.4%, which is still within the elastic range. The color distribution near the fiber crack visualized through an image processing was shown in Fig. 10a. The colors of every pixel related to N values of 2.56, 2.52, and 2.50 were extracted, and then plotted as contours in the rz axis, as shown in Fig. 10b. Three contours were selected for the measurement of t_o. Through application of Eq. 20, these contours were found to be $\Delta\sigma$ values of 10.1, 9.9, and 9.8 MPa, respectively. These $\Delta\sigma$ values must be corrected to compensate for the axisymmetric effect because the carbon fiber has a circular shape that leads to axisymmetry in the projection. The corrected $\Delta\sigma$ (σ_c) can be calculated from [27, 29, 35] as

$$\sigma_c = \frac{h(\Delta\sigma - E_m\varepsilon_a)(b-a)}{2\left\{bm - \frac{1}{2}\left(mb + (a+L_t)^2 ln\frac{(m+b)}{(a+L_t)}\right)\right\}} + E_m\varepsilon_a \,, \quad (21)$$

where m is obtained from

$$m = [b^2 - (L_t - a)^2]^{0.5}. \quad (22)$$

σ_c values of 32.6, 29.3, and 26.9 MPa were obtained from the calculations for the $\Delta\sigma$ values of 10.1, 9.9, and 9.8 MPa, respectively. The L_t, a, and σ_c were measured and substituted into Eq. 19. As a result, the t_o values of 23.4, 29.3, and 31.5 MPa were finally obtained. The same procedure was repeated for 26 other stress contours from three specimens, and resulted in an average value of 23.8 MPa.

A conventional SFFT that considers the interface as being a rigid bond was also conducted for the same specimens. Fig. 11 shows fragmentation process of fiber on initial and saturated conditions. The images were captured without installing retarders on photoelastic tools in order to observe location of fiber cracks. The analysis of conventional SFFT follows Ref. 36 which clearly explain the procedure. The averaged t_o value from the conventional SFFT was 33.7 MPa. The detail comparison of t_o evaluation between our analysis and conventional SFFT analysis is shown in Fig. 12. It is confirmed that t_o is overestimated unless non-rigid bonding is considered. Furthermore, our proposed procedure to evaluate t_o is easier and more straightforward compared to the conventional SFFT, because it requires only measurement of L_t based on the stress response of the matrix to the interface.

Conclusion

A method to evaluate the interfacial strength (t_o) between fiber and matrix has been developed based on the cohesive damage model. The characteristic length (L_t) indicating t_o was introduced and measured from a $\Delta\sigma$ contour in epoxy matrix. Hence, a theoretical analysis was conducted to obtain the relationship between t_o and L_t. From a non-dimensional analysis, it was found that the normalized t_o (t') and L_t (L') have a linear relationship independently determined from material properties. A sample application to carbon fiber-epoxy composite was demonstrated to evaluate the proposed technique. A photoelastic analysis in conjunction with an SFFT experiment was conducted to capture the stress contours, clearly visualized through image processing techniques. The calculated result yielded an average t_o value of 23.8 MPa, which is almost 30% lower than one obtained from conventional SFFT analysis. The overestimation of conventional method implies the importance of debonding process of the interface.

Acknowledgements

This work was financially supported by the Mizuho Foundation for the Promotion of Sciences. The authors thank IRIS Co. Ltd for the cooperation of developing an image processing software.

References

[1] L.J. Broutman, B.D. Agarwal, Effect of the interface on the mechanical properties of composites. Rheol. Acta. 13 (1974) 618–626.

[2] O.I. Okoli, G.F. Smith, Failure modes of fiber reinforced composites: the effects of strain rate and fiber content, J. Mater. Sci. 33 (1998) 5415–5422.

[3] H.L. Cox, The elasticity and strength of paper and other fibrous materials, Brit. J. Appl. Phys. 3 (1952) 72–78.

[4] A. Kelly, W. Tyson, Tensile properties of fiber-reinforced metal: copper/tungsten and copper/molybdenum, J. Mech. Phys. Solids 13 (1965) 329–350.

[5] J.K. Kim, L.M. Zhou, Y.W. Mai, Stress transfer in the fiber fragmentation test, Part I. An improved analysis based on shear strength criterion, J. Mater. Sci. 28 (1993) 6233–6245.

[6] H.D. Wagner, J.A. Nairn, M. Detassis, Toughness of interfaces from initial-matrix debonding in a single fiber composite fragmentation test, Appl. Compos. Mater. 2 (1995) 107–117.

[7] X.F. Zhou, J.A. Nairn, H.D. Wagner, Fiber-matrix adhesion from the single-fiber composite test: nucleation of interfacial debonding, Compos. Part A-Appl. S. 30 (1999) 1387–1400.

[8] S. Kimura, J. Konayagi, H. Kawada, Evaluation of initiation of the interfacial debonding in single-fiber composites (Energy balance method considering an energy dissipation of the plastic deformation), JSME Inter. J. 49 (2006) 451–457.

[9] M. Sharma, S. Gao, E. Mader, H. Sharma, L.Y. Wei, J. Bijwe, Carbon fiber surfaces and composite interphases, Compos. Sci. Technol. 102 (2014) 35–50.

[10] J.J. Lesko, R.E. Swain, J.M Cartwright, J.W. Chin, K.L. Reifsnider, D.A. Dillard, J.P. Wightman, Interphases developed from fiber sizings and their chemical-structural relationship to composite compressive performance, J. Adhesion. 45 (1994) 43–57.

[11] Y. Wang, T. Hahn, AFM characterization of the interfacial properties of carbon fiber reinforced polymer composites subjected to hygrothermal treatments, Compos. Sci. Technol. 67 (2007) 92–101.

[12] D.G. Aggelis, D. Kleitsa, T.E. Matikas, Ultrasonic characterization of the fiber-matrix interfacial bond in aerospace composites, Sci. World J. 154984 (2013) 1–8.

[13] C. Atkinson, On stress singularities and interfaces in linear elastic fracture mechanics, Int. J. Fract. 13 (1977) 807–819.

[14] P. Karpur, T.E. Matikas, S. Krishnamurthy, Ultrasonic characterization of the fiber-matrix interphase/interface for mechanics of continuous fiber reinforced metal matrix and ceramic matrix composites, Compos. Eng. 5 (1995) 697–711.

[15] Y. Leng, T.H. Courtney, Ineffective length in metal matrix composites. Mater. Sci. Eng. A124 (1990) 141–149.

[16] A.I. Beltzer, M. Piau, Y. Weitsman, Note on the ineffective length of a fiber, Mech. Mater. 13 (1992) 285–294.

[17] F. Ma, K. Kishimoto, A continuum interface debonding model and application to matrix cracking of composite. JSME Inter. J. 39A (1996) 496–507.

[18] A. Turon, J. Costa, P. Maimi, D. Trias, J.A. Mayugo, A progressive damage model for unidirectional fibre-reinforced composites based on fiber fragmentation. Part I: formulation. Compos. Sci. Tech. 65 (2005) 2039–2048.

[19] M.A. Minnicino, M.H. Santare, Modelling the progressive damage of the microdroplet test using contact surfaces with cohesive behavior, Compos Sci. Tech.72 (2012) 2024–2031.

[20] N. Chandra, H. Li, C. Shet, H. Ghonem, Some issues in the application of cohesive zone models for metal-ceramic interfaces, Inter. J. Solids Struct. 39 (2002) 2827–2855.

[21] J.H. You, W. Lutz, H. Gerger, A. Siddiq, A. Brendel, A. Hoschen, S. Schmauder, Fiber push-out study of a copper matrix composite with an engineered interface: Experiments and cohesive element simulation, Inter. J. Solids Struct. 46 (2009) 4277–4286.

[22] M. Nishikawa, T. Okabe, K. Hemmi, N. Takeda, Micromechanical modeling of the microbond test to quantify the interfacial properties of fiber-reinforced composites, Inter. J. Solids Struct. 45 (2998) 4098-4113.

[23] M. Nishikawa, T. Okabe, N. Takeda, Determination of interface properties from experiments on the fragmentation process in single-fiber composites, Mater. Sci. Eng. A-Struct. 480 (2008) 549–557.

[24] F.R. Jones, D. Tripathi, Single fiber fragmentation test for assessing adhesion in fibre reinforced composites, J. Mater. Sci. 33(1998) 1–16.

[25] F.M. Zhao, T. Okabe, N. Takeda. The estimation of statistical fiber strength by fragmentation tests of single-fiber composites, Compos. Sci. Technol. 60 (2000) 1965-1974.

[26] B.A. Budiman, K. Takahashi, K. Inaba, K. Kishimoto. A new method of evaluating interfacial properties of a fiber/matrix composite. J. Compos. Mater. 49 (2015) 465–475.

[27] B. Fiedler, K. Schulte, Photo elasticity analysis of fibre reinforced model composite materials, Compos. Sci. Technol. 57 (1997) 859–867.

[28] F.M. Zhao, E.A. Patterson, F.R. Jones. Phase-stepping photoelasticity for quantifying the interfacial response in fiber composites at fibre-breaks. Mater. Sci. Eng. 410 (2005) 83–87.

[29]F.M. Zhao, R.D.S. Martin, S.A. Hayes, E.A. Patterson, R.J. Young, F.R. Jones, Photoelastic analysis of matrix stresses around a high modulus sapphire fiber by means of phase-stepping automated polariscope, Compos. Part A-Appl. S. 36 (2005) 229–244.

[30] T.H. Baek, M.S. Kim, D.P. Hong. Fringe analysis for photoelasticity using image processing techniques. Inter. J. Softw. Eng. and Appl. 8 (2014) 91−102.

[31] P. Zhao, S. Ji, Refinements of shear-lag model and its applications, Tectonophysics. 279 (1997) 37−53.

[32] J.A. Nairn, Y.C. Liu, Stress transfer into fragmented, anisotropic fiber through an imperfect interface, Inter. J. Solids Struct. 34 (1997) 1255–1281.

[33] S.V. Nair, H.G. Kim, Modification of the shear lag analysis for determination of elastic modulus of short-fiber (or whisker) reinforced metal matrix composites, J. Appl. Mech. 59 (1992) 176-182.

[34] A. Ajovalasit, G. Petrucci, M. Scafidi, Review of RGB Photoelasticity. Optics and Lasers Engineering, 68 (2015) 58-73.

[35] B.M. Schuster, B. Scala, The mechanical interaction of sapphire whiskers with a birefringent matrix. T. Metal. Soc. AIME. 230 (1964) 1635–1640.

[36] J. M. Rich, L. T. Drzal, Round robin assessment of the single fiber fragmentation test. Proceedings of The American Society for Composites 17th Technical Conference. Indiana, 21-23 October 2002, pp 1-10. Gaitherburg: NIST.

Figure Legends

Fig. 1. Fiber fragmentation process; (a) before and (b) after.

Fig. 2. Shear traction (t_s)-separation (δ_s) curve.

Fig. 3. Axisymmetric model of fiber/matrix composite near fiber crack.

Fig. 4. FEA result for carbon fiber-hard epoxy composite with case-1 interfacial properties: (a) t_s and dt_s/tz curves along simulated interface; (b) $\Delta\sigma$ contours in matrix. The black dots indicate the maximum radius (r_{max}) with respect to the r-axis.

Fig. 5. Measurement of t_o for carbon fiber-hard epoxy composite. The black and white marks indicate measurements with and without considering dt_s/dz respectively.

Fig. 6. Measurement of t_o for glass fiber-soft epoxy composite. The black and white marks indicate measurements with and without considering dt_s/dz respectively.

Fig. 7. Linear relationship approximation between *t'* and *L'*.

Fig. 8. Schematic of apparatus used for photoelastic analysis.

Fig. 9. (a) colored band observed under bending load and (b) epoxy stress-fringe order curve.

Fig. 10. (a) color captured near fiber crack using photoelastic technique and (b) plotted $\Delta\sigma$ contours from experiment.

Fig. 11. Fiber cracks appearance on SFFT (a) initial and (b) saturated conditions.

Fig. 12. Comparison of t_o evaluation between conventional SFFT and our experimental analysis.

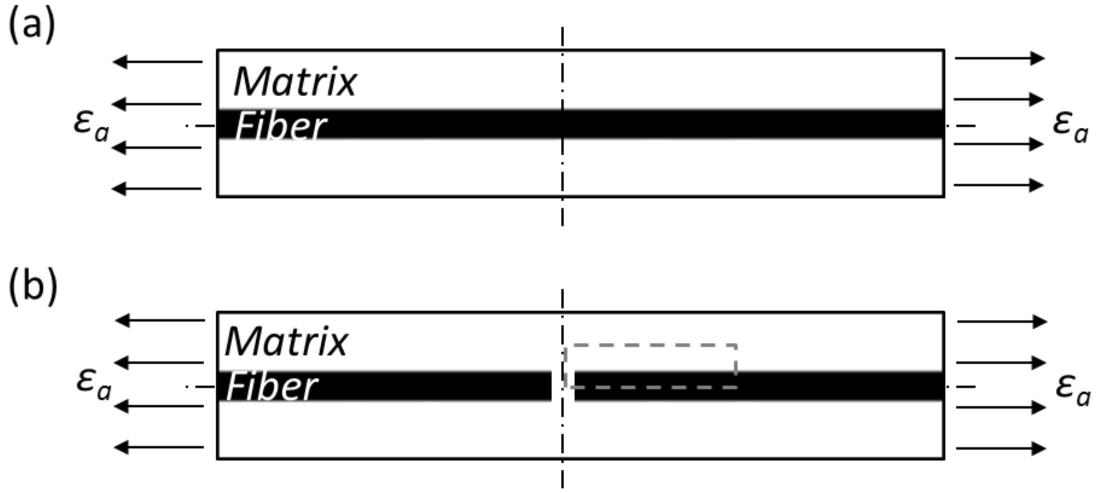

Fig. 1. Fiber fragmentation process; (a) before and (b) after.

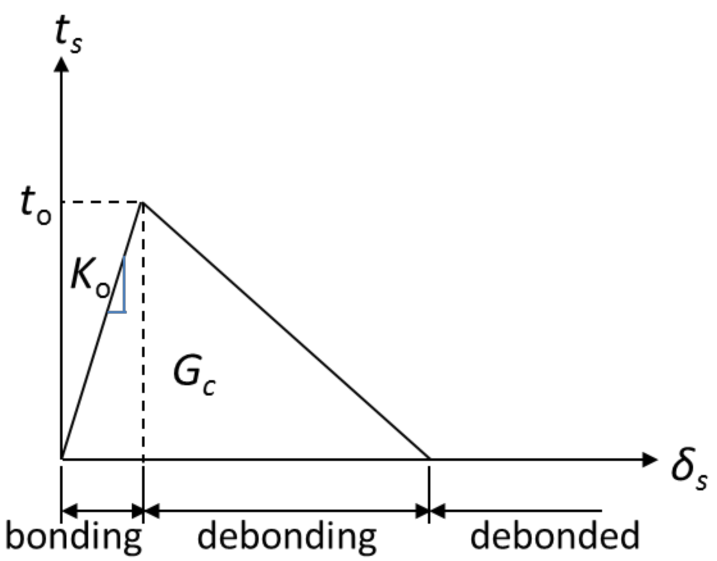

Fig. 2. Shear traction (t_s)-separation (δ_s) curve.

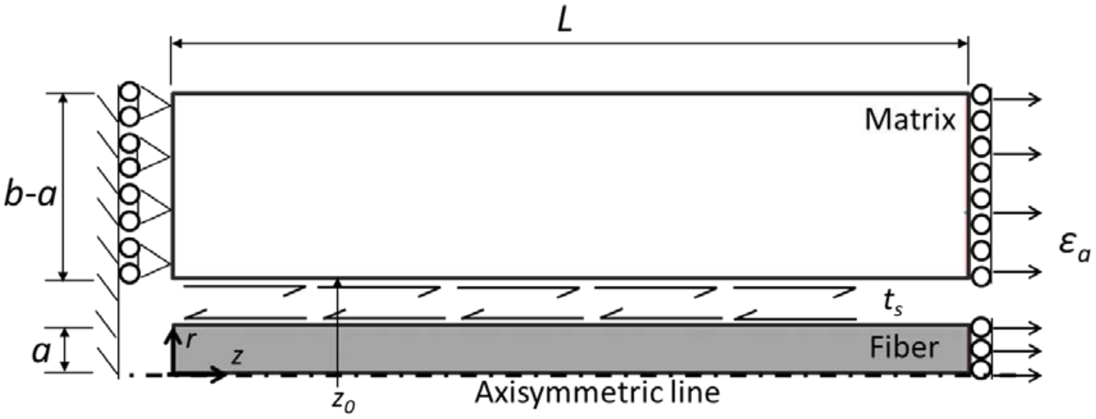

Fig. 3. Axisymmetric model of fiber/matrix composite near fiber crack.

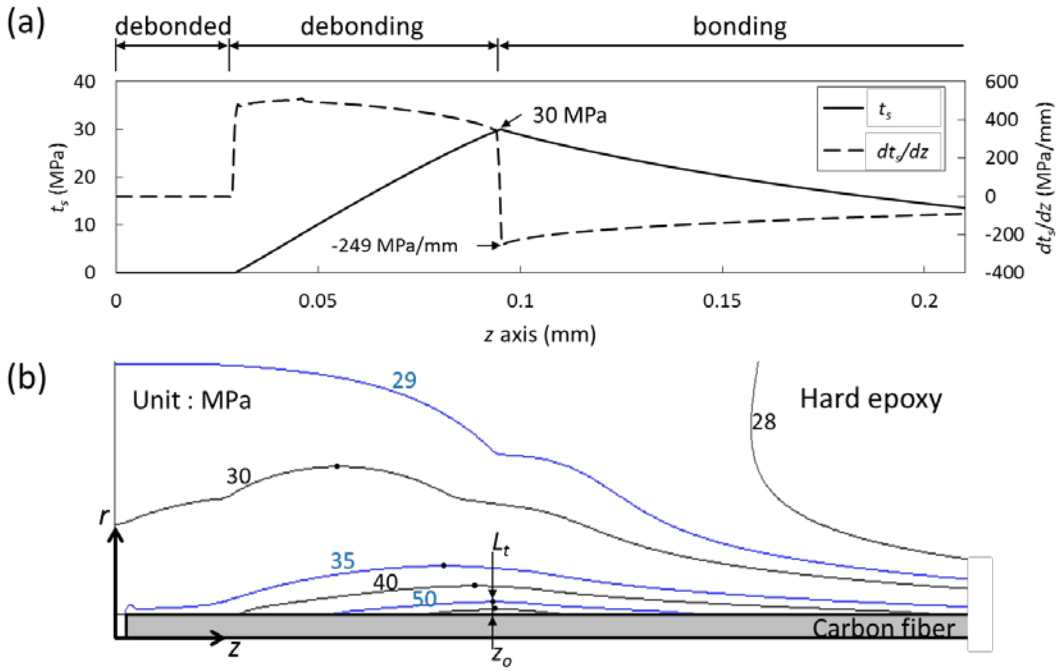

Fig. 4. FEA result for carbon fiber-hard epoxy composite with case-1 interfacial properties: (a) t_s and dt_s/tz curves along simulated interface; (b) $\Delta\sigma$ contours in matrix. The black dots indicate the maximum radius (r_{max}) with respect to the *r*-axis.

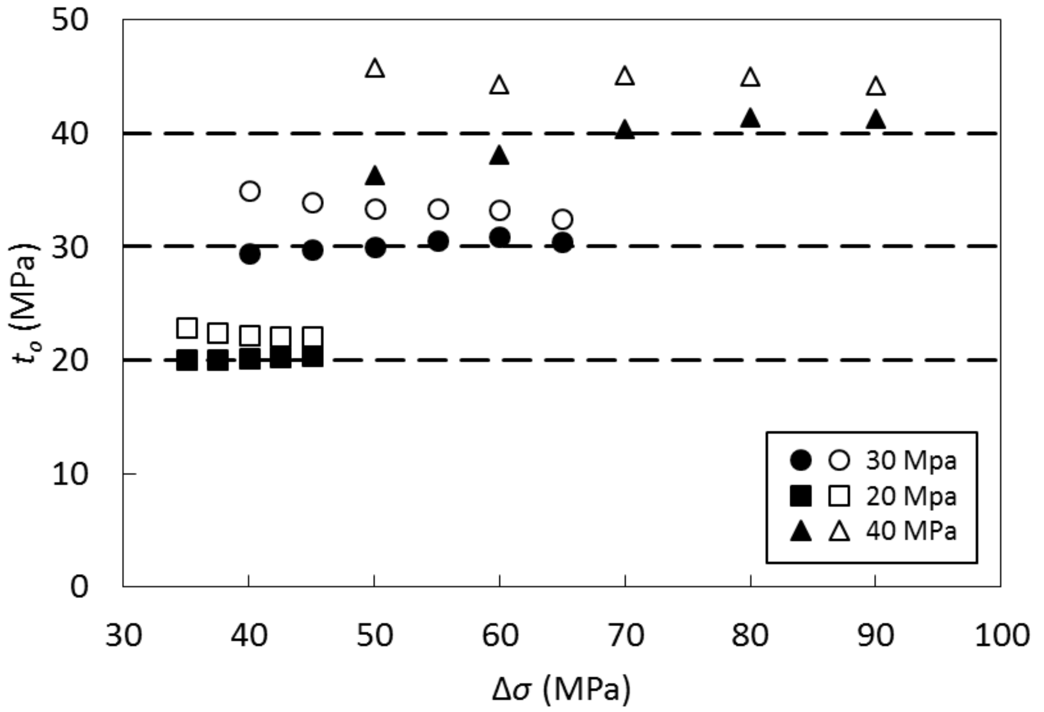

Fig. 5. Measurement of t_o for carbon fiber-hard epoxy composite. The black and white marks indicate measurements with and without considering dt_s/dz respectively.

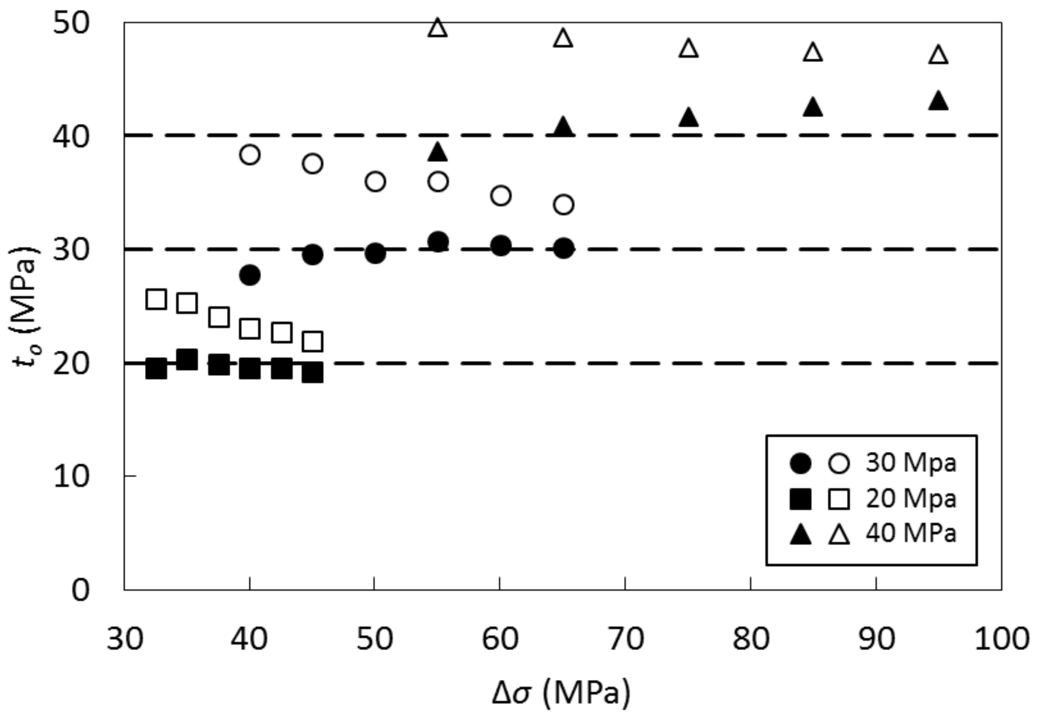

Fig. 6. Measurement of t_o for glass fiber-soft epoxy composite. The black and white marks indicate measurements with and without considering dt_s/dz respectively.

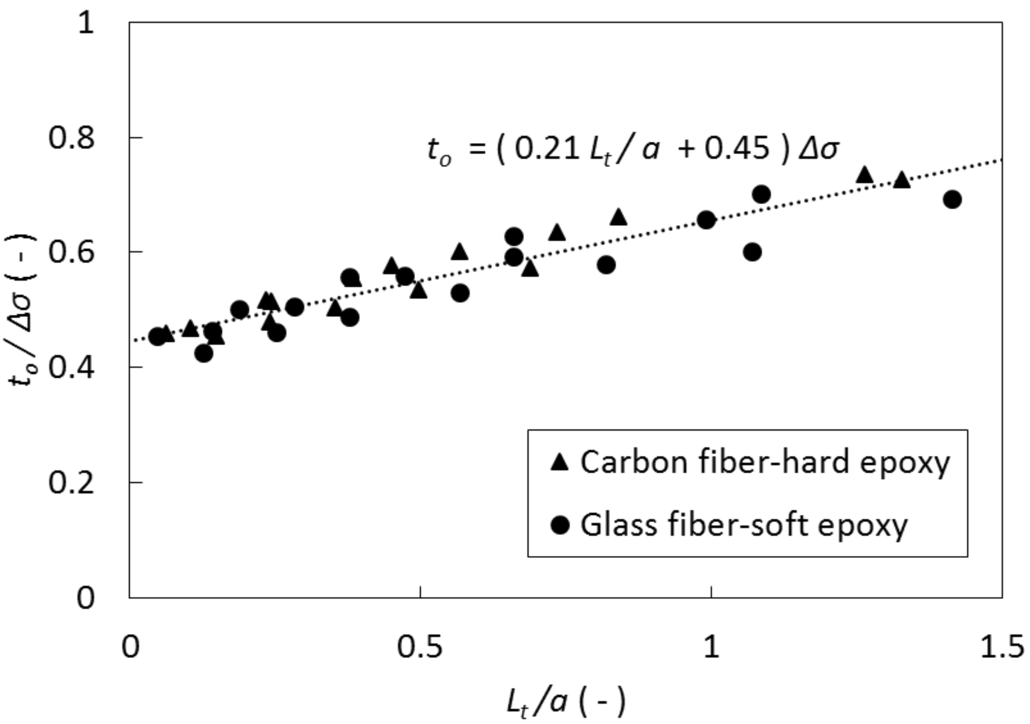

Fig. 7. Linear relationship approximation between *t'* and *L'*.

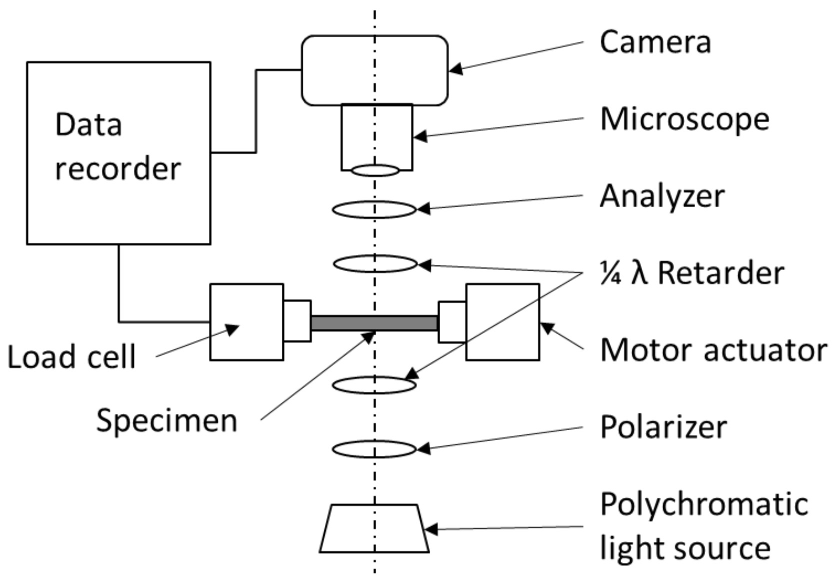

Fig. 8. Schematic of apparatus used for photoelastic analysis.

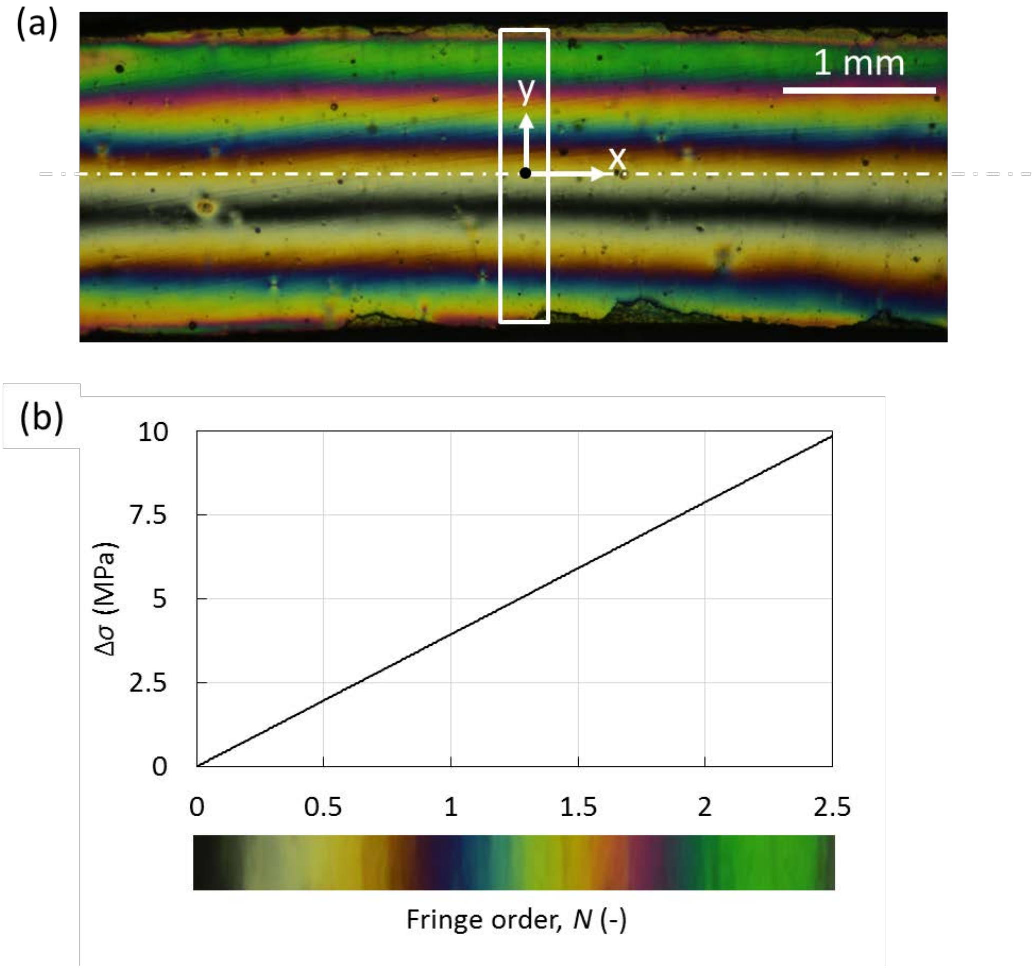

Fig. 9. (a) Colored band observed under bending load and (b) epoxy stress-fringe order curve.

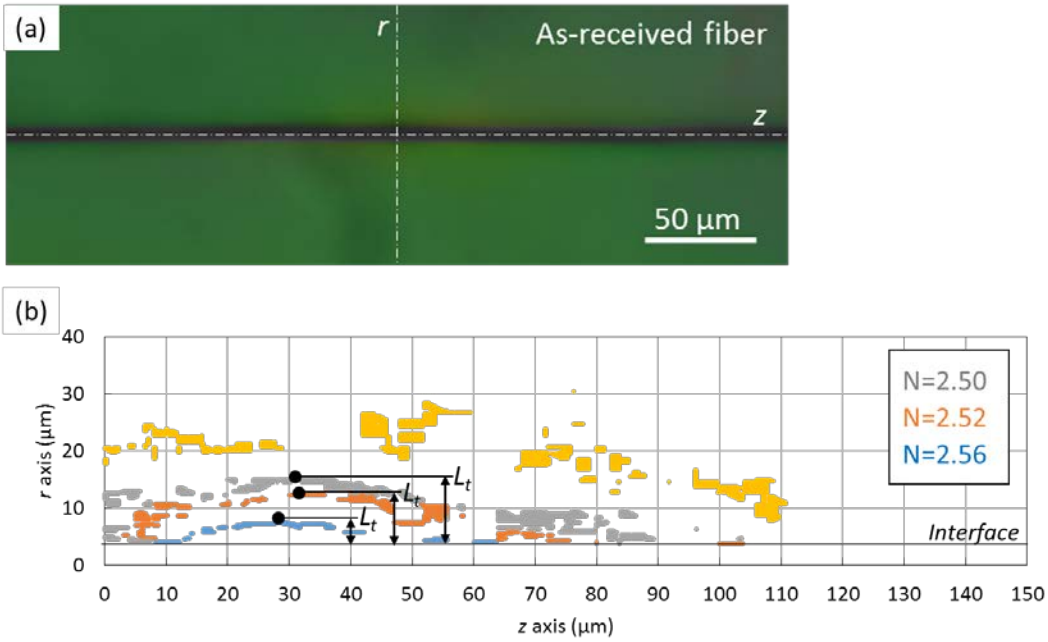

Fig. 10. (a) color captured near fiber crack using photoelastic technique and (b) plotted $\Delta\sigma$ contours from experiment.

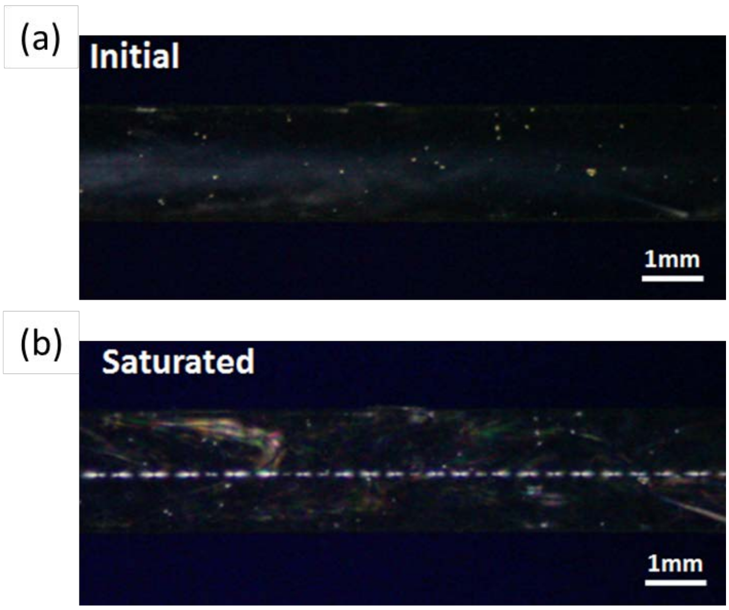

Fig. 11. Fiber cracks appearance on SFFT (a) initial and (b) saturated conditions

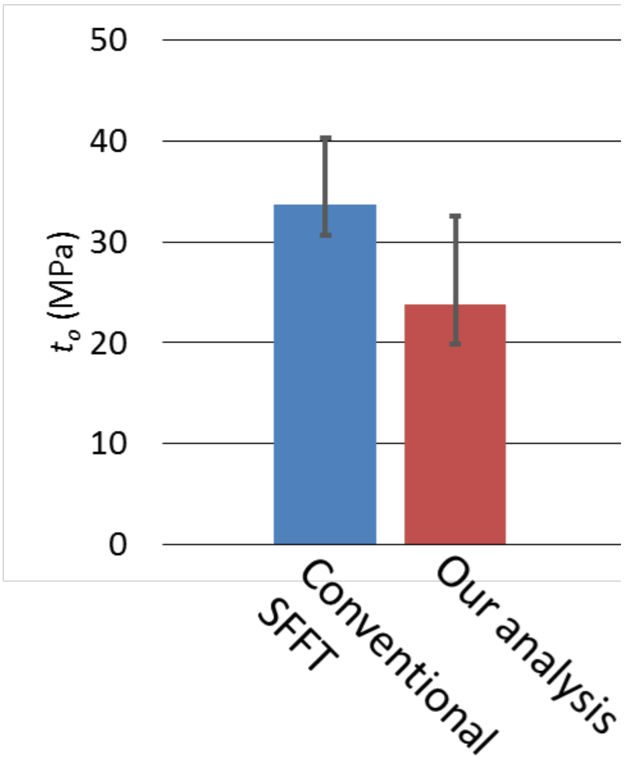

Fig. 12. Comparison of t_o evaluation between conventional SFFT and our experimental analysis.

Table 1. Mechanical properties of fibers and epoxy used in simulations.

Parameter	Elastic modulus (E)	Poisson ratio (ν)
Carbon fiber[a]	240 GPa	0.2
Glass fiber[b]	80 GPa	0.22
Hard epoxy[c]	2 GPa	0.4
Soft epoxy[c]	1 GPa	0.4

[a]Toho Tenax`s Datasheet, [b]ASM handbook vol 21: Composites, [c]assumption

Table 2. Model parameters used in simulation.

Parameter	Value
Fiber radius (a)	3.5 µm
Matrix radius (b)	70 µm
Model length (L)	1 mm
Fiber element	10500 els. (7×1500)
Matrix element	82500 els. (55×1500)

Table 3. Interfacial properties of sample cases examined via simulation.

Interfacial properties	Case 1	Case 2	Case 3
Interfacial stiffness (K_o)	2×10^4 MPa/mm	2×10^4 MPa/mm	2×10^4 MPa/mm
Interfacial strength (t_o)	30 MPa	20 MPa	40 MPa
Interfacial fracture toughness (G_c)	0.04 mJ/mm^2	0.03 mJ/mm^2	0.05 mJ/mm^2